Inorganic Chemistry

Article

pubs.acs.org/IC

Structure Induced Yb Valence Changes in the Solid Solution $Yb_xCa_{1-x}C_2$

Pascal Link,[†] Pieter Glatzel,[‡] Kristina Kvashnina,[‡] Dmytro M. Trots,[§] Ronald I. Smith,[∥] and Uwe Ruschewitz*,[†]

[†]Department of Chemistry, University of Cologne, Greinstrasse 6, D-50939 Cologne, Germany

[‡]European Synchrotron Radiation Facility, BP 220, 6 rue Horowitz, F-38043 Grenoble, France

[§]Hamburg Synchrotron Radiation Facility HASYLAB/DESY, D-22607 Hamburg, Germany

[∥]ISIS Facility, Rutherford Appleton Laboratory, Chilton, Didcot, Oxfordshire OX11 0QX, United Kingdom

Supporting Information

ABSTRACT: The solid solution $Yb_xCa_{1-x}C_2$ ($0 \leq x \leq 1$) was synthesized by reaction of the elements at 1323 K. The crystal structures within this solid solution, as elucidated from synchrotron powder diffraction data, depend on x and exhibit some interesting features that point to a structure dependent valence state of Yb. Compounds with $x \geq 0.75$ crystallize in the tetragonal CaC_2 type structure ($I4/mmm$, $Z = 2$) and obey Vegard's law; for $x \leq 0.75$ the monoclinic ThC_2 type structure ($C2/c$, $Z = 4$) is found, which coexists with the monoclinic CaC_2-III type structure ($C2/m$, $Z = 4$) for $x \leq 0.25$. The monoclinic modifications show a strong deviation from Vegard's law. Their unit cell volumes are remarkably larger than expected for a typical Vegard system. HERFD-XANES spectroscopic investigations reveal that different Yb valence states are responsible for the observed volume anomalies. While all tetragonal compounds contain mixed-valent Yb with ~75% Yb^{3+} (similar to pure YbC_2), all monoclinic modifications contain exclusively Yb^{2+}. Therefore, $Yb_xCa_{1-x}C_2$ is a very rare example of a Yb containing compound showing a strong structure dependence of the Yb valence state. Moreover, temperature dependent synchrotron powder diffraction, neutron TOF powder diffraction, and HERFD-XANES spectroscopy experiments reveal significant Yb valence changes in some compounds of the $Yb_xCa_{1-x}C_2$ series that are induced by temperature dependent phase transitions. Transitions from the tetragonal CaC_2 type structure to the monoclinic ThC_2 or the cubic CaC_2-IV type structure ($Fm\bar{3}m$, $Z = 4$) are accompanied by drastic changes of the mean Yb valence from ~2.70 to 2.0 in compounds with $x = 0.75$ and $x = 0.91$. Finally, the determination of lattice strain arising inside the modifications with ordered dumbbells (ThC_2 and CaC_2 type structures) by DSC measurements corroborated our results concerning the close relationship between crystal structure and Yb valence in the solid solution $Yb_xCa_{1-x}C_2$.

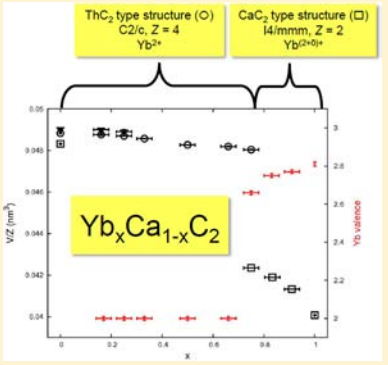

INTRODUCTION

Valence changes in lanthanide containing compounds, induced by changes in pressure, temperature, or the chemical and geometric surrounding of the lanthanide metal cation, are of great interest in both chemistry and physics. They often lead to interesting physical effects like the Kondo effect or heavy fermion behavior and sometimes cause dramatic changes of physical properties such as electrical resistivity or magnetic susceptibility, which makes them valuable for technical applications. Numerous lanthanide containing compounds showing different kinds of valence changes are known today.[1−7] However, most of them are intermetallic compounds; nonintermetallics are quite rare with YbS[5] being the most prominent representative. Quite recently it was found that the fullerides $Ln_{2.75}C_{60}$ (Ln = Sm,[8] Yb[9]) show an extremely high negative thermal lattice expansion at low temperatures. It was found that a valence change from $Ln^{(2+\delta)+}$ to Ln^{2+} is responsible for this unusual behavior.

Looking at the lanthanide dicarbides LnC_2 (Ln = lanthanide metal), EuC_2 and YbC_2 could be another class of non-intermetallic compounds showing interesting valence effects. Both compounds have been known for decades, but their crystal structures and cation valences have been discussed contradictorily in the literature.[10−15] Very recently we showed that EuC_2 crystallizes in the monoclinic ThC_2 type structure ($C2/c$, $Z = 4$) in contrast to all other lanthanide dicarbides LnC_2, which crystallize in the tetragonal CaC_2 type structure ($I4/mmm$, $Z = 2$).[10,12,16] Furthermore, Mössbauer spectroscopic investigations and magnetization measurements revealed that the Eu cation is in a divalent state in EuC_2, whereas all other LnC_2 compounds contain trivalent lanthanide metal cations.[13,15,16] YbC_2 crystallizes in the tetragonal CaC_2 type structure as all other LnC_2 compounds,[10] but its unit cell volume is slightly larger than expected from the lanthanide

Received: February 28, 2013
Published: May 30, 2013

   dx.doi.org/10.1021/ic400531j | Inorg. Chem. 2013, 52, 7020−7030

contraction. Our recent work on YbC_2 clearly showed that a mixed valence state of Yb is responsible for this enhanced unit cell volume.[17] HERFD-XANES spectroscopic investigations resulted in a mean Yb valence of ~2.81,[17] which basically confirms the results obtained by other groups in the past.[18,19]

These findings suggested that both EuC_2 and YbC_2 might be possible candidates for exhibiting changes of the cation valence states induced by temperature, pressure, or a variation of the chemical/geometric surrounding. Actually, a valence change in these compounds could be of particular interest, as the trivalent state leads to metallic behavior, whereas for the divalent state in EuC_2 semiconducting behavior was found.[11,15,16] Thus, a change of the valence state of the cation in EuC_2 and YbC_2 should lead to a drastic change of its electronic properties. But up to now we could not find any temperature dependent change of the Eu or Yb valence in EuC_2 and YbC_2. Our recent investigations on YbC_2 using HERFD-XANES spectroscopy clearly showed that the Yb valence remains constant over a wide temperature range (15−1123 K),[17] which is in contrast to previous work of other groups, who suggested a strongly temperature dependent fluctuation of the Yb valence.[20] The influence of pressure on the Eu valence in EuC_2 is subject of our current research and will be discussed elsewhere.

Recently, we have started to study the influence of the surrounding of the lanthanide cation on its valence state by synthesizing solid solutions composed of LnC_2 and alkaline earth metal carbides AEC_2 (AE = alkaline earth metal). This idea was triggered by the observation that EuC_2 with divalent Eu crystallizes in the monoclinic ThC_2 type structure, whereas all other LnC_2 compounds with trivalent Ln crystallize in the tetragonal CaC_2 type structure. YbC_2, in which Yb is close to a trivalent state, also fits nicely into this simple picture. This suggests a structure dependence of the lanthanide metal valence. As alkaline earth metal carbides AEC_2 show a pronounced polymorphism with different crystal structures coexisting at room temperature,[21−23] we expected a similar polymorphism for solid solutions of composition $Ln_xAE_{1-x}C_2$ as a function of x. Thus, the geometric surrounding of the lanthanide cation can be changed systematically, and the influence of these structural changes on the valence state of the cation may be investigated. Additionally, the introduction of divalent alkaline earth metal cations into the LnC_2 lattice will further result in a direct change of the chemical surrounding of the lanthanide metal cation, which might also influence the valence state of the lanthanide.

The first system we investigated was $Eu_xSr_{1-x}C_2$ with $0 \le x \le 1$.[24] As Eu^{2+} (135 pm, CN = 10) and Sr^{2+} (136 pm, CN = 10) have very similar ionic radii,[25] the formation of a solid solution was very likely. Indeed, we obtained a strain free solid solution showing perfect Vegard behavior. As expected the system showed a pronounced polymorphism as a function of x. For $x > 0.5$ only the monoclinic ThC_2 type structure was found, whereas for $x \le 0.5$ the ThC_2 type structure coexists with the tetragonal CaC_2 type structure. However, the change of the crystal structure from monoclinic (like obtained for pure EuC_2) to tetragonal did not result in a change of the Eu valence state. This was investigated by Mössbauer spectroscopy, which showed the exclusive presence of Eu^{2+} cations for the whole composition range.[24]

In this current Article we report the results of our investigations on the solid solution $Yb_xCa_{1-x}C_2$ with $0 \le x \le 1$. This time we have chosen calcium as the alkaline earth metal, as the ionic radius of Yb^{2+} (112 pm, CN = 10) is very similar to that of Ca^{2+} (114 pm, CN = 10).[25] However, the Yb cation in YbC_2 resides in a mixed-valent state with an average valence of ~2.81, which is close to 3. Thus, the introduction of larger Ca^{2+} ions into the YbC_2 lattice should produce a significant lattice strain that might be reduced by a change of the Yb valence from 2.81 to 2. On the other hand, it was not straightforward that a successful synthesis of a complete solid solution $Yb_xCa_{1-x}C_2$ with $0 \le x \le 1$ is feasible, as there is a 17% difference between the normalized cell volumes ($\Delta V_n/V_n$ with $V_n = V/Z$) of YbC_2 and CaC_2. The synthesized compounds have been analyzed by synchrotron and neutron powder diffraction techniques to clarify their crystal structures. HERFD-XANES spectroscopy was used to obtain the Yb valence state. Finally, DSC measurements have been performed to gather information about the lattice strain in this solid solution.

EXPERIMENTAL DETAILS

General Remarks. Due to the high sensitivity of Yb, Ca, YbC_2, and CaC_2 to moisture and oxygen, all sample handling was carried out in an inert atmosphere (Ar, 99.999%). Yb metal pieces were obtained from Chempur (distilled, 99.99%) and Ca metal pieces from Sigma-Aldrich (99.99%). Both metals were filed to small chips in a glovebox (argon atmosphere). Prior to the reaction, graphite (Aldrich, 99.9998%) was heated to 1070 K for 48 h in a dynamic vacuum and stored in an argon atmosphere.

Sample Preparation. All compounds of the solid solution $Yb_xCa_{1-x}C_2$ were prepared by reaction of the elements at high temperatures inside a tantalum bomb in an inert atmosphere. In a typical reaction 173.0 mg of Yb chips (1 mmol), 40.0 mg of Ca chips (1 mmol), and 49.2 mg of graphite (4.1 mmol) were mixed in a shallow shell. A small surplus of graphite was chosen ((Yb + Ca):C = 1:2.05) to inhibit the formation of Yb_2O_3 with oxygen impurities and to account for graphite losses due to a reaction with the container wall. The resulting mixture was transferred into a surface cleaned Ta ampule that was sealed in an arc furnace (helium atmosphere, 800 mbar, 10 A). The ampule was subsequently encapsulated into a silica tube under vacuum to avoid the oxidation of the Ta metal at high temperatures. The resulting reaction container was heated in a high temperature furnace (HTRH, GERO Hot Solutions) at 1323 K (heating rate 250 K/h) for 24 h and cooled down by switching off the furnace.

Structural Investigations. High-temperature synchrotron powder investigations (298−1148 K) were performed at the powder diffractometer of beamline B2 of the Hamburg synchrotron facility (HASYLAB) using the following setup: λ = 49.901 pm or λ = 65.133 pm; position sensitive imaging plate detector system (OBI[26]); STOE capillary furnace. The exposure time of each diffraction pattern (approximately 15 min) was corrected for fluctuations and decay of the synchrotron beam by using monitor counts collected between the incident beam and the sample. The sample was sealed in a silica glass capillary (⌀ = 0.3 mm) under argon. The actual temperature of the furnace was obtained from the temperature dependence of the lattice parameter of NaCl, which was measured as a standard prior to the measurements of the title compounds. The set point temperatures of the furnace were corrected accordingly. All diffractograms were analyzed using the STOE software WinXPOW.[27] For the Rietveld refinements the GSAS software package was applied.[28] To obtain a reliable trend of the lattice parameters and molar ratios of the different modifications the same sets of variables were used in the final Rietveld refinements of all diffractograms of one sample.

Time-of-flight (TOF) powder neutron diffraction data were collected on the POLARIS beamline at the ISIS pulsed spallation source (Rutherford Appleton Laboratory, U.K.).[29] Approximately 4 g of $Yb_xCa_{1-x}C_2$ was loaded into a thin-walled cylindrical vanadium sample can (⌀ = 6 mm, height ≈ 50 mm, wall thickness ≈ 0.15 mm) inside a glovebox (argon atmosphere). The can was sealed with indium wire. Diffraction patterns were collected for ~100 μAh (integrated proton beam current to the ISIS target, corresponding to ~40 min data collection time) at room temperature and between 5 and 100 K in

dx.doi.org/10.1021/ic400531j | Inorg. Chem. 2013, 52, 7020−7030

5 K steps using an AS Scientific "orange" helium cryostat. The cryostat and sample temperatures were monitored and controlled using RhFe temperature sensors connected to Eurotherm 3504 controllers. Data collected in three detector banks centered at $2\theta = 145°$ ($d_{max} = 3.2$ Å), $2\theta = 90°$ ($d_{max} = 4.2$ Å), and $2\theta = 35°$ ($d_{max} = 8.2$ Å) were normalized and corrected for absorption prior to crystal structure refinement. Full profile refinement by the Rietveld method was carried out with the GSAS software package.[28]

X-ray Spectroscopy. X-ray absorption near edge structure (XANES) spectra at the Yb L_{III} edge were recorded at beamline ID26 of the European Synchrotron Radiation Facility (ESRF) in Grenoble, France.[30] The data were collected using high energy resolution fluorescence detection (HERFD-XANES) by means of an X-ray emission spectrometer. The incident energy was selected using the ⟨311⟩ reflection from a double Si crystal monochromator. The incident flux was 5×10^{12} photons/second with a beam size on the sample of 1.0×0.2 mm^2 (horizontal × vertical). Subsequently, the fluorescence radiation of the sample was reflected by a Si ⟨620⟩ crystal analyzer, focusing the Yb $L\alpha_1$ line on a photon detector (avalanche photodiode). Sample, analyzer crystal and detector were arranged in a vertical Rowland geometry. Conventional XANES spectra in total fluorescence yield (TFY) were detected simultaneously by using a photodiode. The fluorescence signal was normalized to the incident flux. Two different set-ups were used to collect data at low and high temperatures: (i) closed-cycle helium cryostat for low temperature investigations (15−300 K) and (ii) high temperature furnace for measurements between 300 and 1200 K. In both set-ups, temperature steps of 30 K were used. To achieve thermal equilibrium, in all measurements the samples were kept at the desired temperature for 15 min and were subsequently measured for about 20 min. For the low temperature measurements, samples were loaded in Lindemann glass capillaries (⌀ = 0.5 mm), while quartz capillaries (⌀ = 0.3 mm) were used for the high temperature measurements. The capillaries were filled in a glovebox (argon atmosphere) and sealed airtight with a heated wire. All spectra were analyzed and normalized using the program ATHENA of the IFEFFIT software package.[31] Subsequent least-squares fitting procedures were carried out with the program GNUPLOT.[32]

Differential Scanning Calorimetry (DSC). DSC measurements were carried out using a Netzsch DTA 404 PC/4/H Eos differential thermal analyzer. Approximately 10−15 mg of the sample was weighed into an alumina crucible, which was closed with a tightly fitting lid within a glovebox. Subsequently, this crucible was heated with a reference crucible made from the same material to 873 K in an argon stream with a heating rate of 10 K/min. Afterward the furnace was cooled down to room temperature with a cooling rate of 10 K/min. This thermal treatment was repeated to check for reversibility. The heat flow between the sample and the reference was obtained by integration of the $\Delta(T - T_{ref})$ curve. To ensure that no oxidation occurs during sample handling and measurement, for each composition two different samples were measured. All data were analyzed with the program NETZSCH Proteus.[33]

RESULTS AND DISCUSSION

Structural Investigations at Room Temperature. Despite the large relative volume difference of YbC_2 and CaC_2 ($\Delta V_n/V_n = 17\%$) we were able to synthesize a complete solid solution series $Yb_xCa_{1-x}C_2$ with $0 \le x \le 1$. The successful synthesis of 10 compounds with differing x (including pure YbC_2 and CaC_2) was clearly proven by synchrotron powder diffraction data. All compounds are obtained as microcrystalline powders with differing colors that depend on the composition x. Compounds with $0 \le x < 0.75$ are black, for $x = 0.75$ an auburn color is found, whereas compounds with $0.75 < x \le 1$ show a golden luster. As usual for lanthanide and alkaline earth metal carbides[12,21] all compounds show a high sensitivity to moisture.

For all compounds synchrotron X-ray powder diffraction data were recorded due to their improved resolution and small absorption using short wavelengths ($\lambda = 49.901$ pm and $\lambda = 65.133$ pm, respectively). The resulting patterns were first indexed, and subsequently, the crystal structures refined by the Rietveld method to get reliable cell constants and ratios of the different modifications. The known crystal structures of YbC_2 and CaC_2 were used as starting models for the refinements.[17,21] Figure 1 shows the refinement of $Yb_{0.75}Ca_{0.25}C_2$ at 295 K as an example for the quality of the data and the refinement.

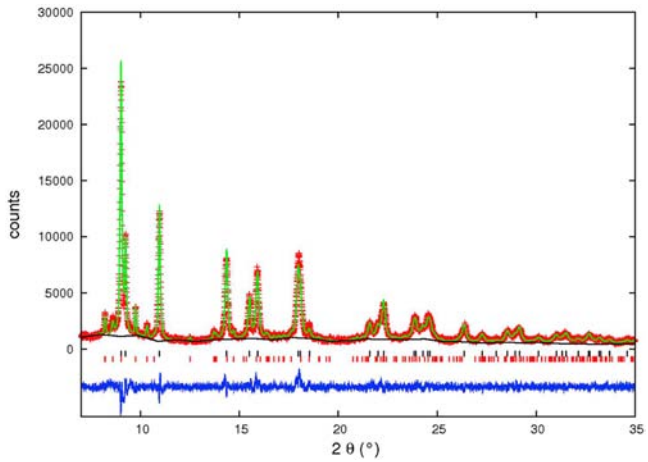

Figure 1. Rietveld refinement of $Yb_{0.75}Ca_{0.25}C_2$ (295 K, $\lambda = 49.901$ pm, HASYLAB/B2) showing the observed (red +) and calculated patterns (green line) as well as the difference between both (blue line). The calculated background is displayed as a black line. Vertical bars mark the positions of the reflections of the CaC_2 type structure (black upper bars) and the ThC_2 type structure (red lower bars).

In all final refinements the composition x (that means the occupancy of the mixed metal sites with Yb and Ca, respectively) has not been refined, as it led to physically meaningless results in most cases. Instead, the composition was taken from the ratio of the starting materials Yb and Ca. Neutron diffraction data described below confirm the validity of this assumption. The inaccuracy of weighing was taken into account by applying an error of ±0.03 to all compositions. Furthermore, atomic positions and displacement parameters of C were not refined as the scattering power of C is too low compared with Yb or Ca to obtain reliable results. Instead, the atomic parameters of C in YbC_2 and CaC_2 were used, and U_{iso} was fixed to 400 pm^2. The refinements revealed minor impurity phases of Yb_2O_3 in some of the samples. However, these impurities did not exceed a mass fraction of 3%. They are therefore neglected in the following discussion. Details of the refinement of $Yb_{0.75}Ca_{0.25}C_2$, representative for all other compounds, are presented in Table 1. Additional diffraction patterns are given in the Supporting Information (Figures S1 and S6) as well as more structural information (Table S1).

As expected, the crystal structures of the compounds highly depend on the composition x (Figure 2). For $x \ge 0.75$ the tetragonal CaC_2 type structure is the only observable phase at room temperature (RT). For $x \le 0.75$ the monoclinic ThC_2 type structure, known as the stable RT modification of CaC_2,[21] is found. This phase coexists for $x \le 0.25$ with the monoclinic CaC_2-III type structure, a crystal structure that was described as being metastable for pure CaC_2.[21,34] Looking at the normalized cell volume V/Z, it is striking that all tetragonal compounds are

dx.doi.org/10.1021/ic400531j | Inorg. Chem. 2013, 52, 7020−7030

Table 1. Selected Structural Parameters of $Yb_{0.75}Ca_{0.25}C_2$ at Room Temperature (Rietveld Refinement, Synchrotron Radiation, λ = 49.901 pm, HASYLAB/B2)

	ThC_2 type structure	CaC_2 type structure
space group, Z	$C2/c$ (No. 15), 4	$I4/mmm$ (No. 139), 2
a/pm	661.8(2)	369.80(2)
b/pm	416.09(9)	
c/pm	728.0(2)	619.35(2)
β/deg	106.53(2)	
V/nm^3	0.19219(5)	0.084 698(6)
Yb/Ca[a]	4e with y = 0.185(4)	2a
U_{iso}/pm^2	100[b]	40(10)
C	not refined[c]	not refined[c]
no. reflns	174	34
R_{Bragg}	0.0371	0.0193
mass fraction/%	10.8(2)	89.13(2)
R_P	0.0954	0.0954
wR_P	0.0778	0.0778
no. refined params	41	41

[a] U_{iso} and atomic positions of metal ions have been constrained. [b] U_{iso} fixed due to small fraction of the phase. [c] See text.

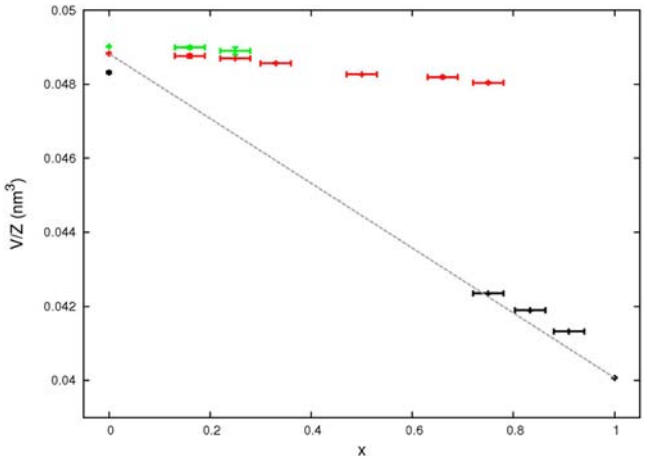

Figure 2. Unit cell volume per formula unit of the different modifications of $Yb_xCa_{1-x}C_2$ as a function of x: monoclinic ThC_2 type structure (red), tetragonal CaC_2 type structure (black), monoclinic CaC_2-III type structure (green). A behavior according to Vegard's law is indicated by a dotted straight line.

in agreement with Vegard's law: their normalized cell volumes are in line with the cell volumes of pure CaC_2 and YbC_2. In contrast, the monoclinic compounds are not in agreement with Vegard's law, as their cell volumes are much larger than expected (Figure 2). This difference between tetragonal and monoclinic compounds can most strikingly be seen in $Yb_{0.75}Ca_{0.25}C_2$, where CaC_2 and ThC_2 type structures coexist at RT. The difference between the normalized cell volumes of these two phases is 5.69 × 10^{-3} nm^3, which corresponds to a relative difference of 12%. In pure CaC_2, which also shows a coexistence of both structure types, the relative volume difference is only 1%. Thus, it can be assumed that different valence states of Yb are a possible reason for this large volume difference, as the Yb^{2+} cation is significantly larger than the Yb^{3+} cation.

HERFD-XANES Spectroscopy at Room Temperature. To clarify the reason for the large volume differences between monoclinic and tetragonal compounds, HERFD-XANES spectroscopic measurements were performed at beamline ID26 of the ESRF. As we already showed for YbC_2, HERFD-XANES spectroscopy is an ideal tool to determine the valence state of lanthanide cations in dicarbide compounds.[17] We therefore collected spectra of all synthesized $Yb_xCa_{1-x}C_2$ compounds to prove the supposed correlation between cell volume and lanthanide metal valence state in this solid solution.

The spectra of five compounds, representative for the whole series, compared with the reference compound Yb_2O_3 are shown in Figure 3. As discussed elsewhere Yb_2O_3 shows a

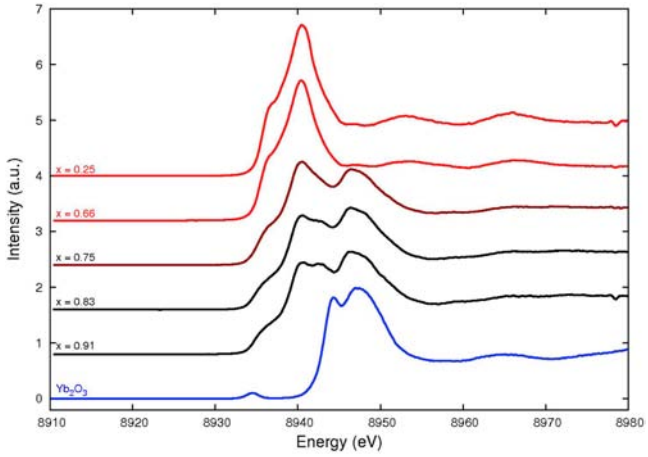

Figure 3. Yb L_{III} HERFD-XANES spectra of five compounds of the solid solution $Yb_xCa_{1-x}C_2$ compared with the trivalent reference compound Yb_2O_3. Monoclinic compounds are displayed in red, tetragonal compounds in black. The dark red color of $Yb_{0.75}Ca_{0.25}C_2$ indicates the coexistence of tetragonal and monoclinic phases at room temperature.

distinct splitting of the trivalent white line at ~8947 eV that cannot be resolved in conventional TFY spectra.[17,35] In an empirical approach it may be satisfactorily described by three Gaussian functions. In contrast, the monoclinic compounds $Yb_xCa_{1-x}C_2$ with $x \leq 0.66$ show a single white line at ~8940 eV without any visible splitting. Compared to Yb_2O_3 this white line is shifted to lower energies by ~7 eV. As the white lines of Yb^{2+} and Yb^{3+} ions generally differ by ~8 eV it seems to be justified to assign different valence states to these two white lines. Thus, the monoclinic compounds contain divalent Yb, as predicted from their unit cell volumes. Consequently, compounds with $x \geq 0.75$ show a mixed-valent behavior, as their HERFD-XANES spectra contain both white lines in different amounts. A similar interpretation of high-resolution Yb L_{III} XANES spectra has already been used by others; e.g., Yamaoka et al. obtained similar spectra for the intermetallic compounds $YbGa_{1.15}Si_{0.85}$ and $YbGa_xGe_{2-x}$.[7]

In general, all Yb L_{III} HERFD-XANES spectra of the solid solution look very different from that of the reference compound Yb_2O_3 (Figure 3). To quantify the Yb valence state as a function of the composition we carried out least-squares fittings to extract the relative intensities of both white lines from the recorded spectra. The exact fitting procedure has already been described elsewhere[17] (see also Figure S15 and Table S2 in the Supporting Information). The results of the fits, directly compared with the unit cell volumes of the compounds, are shown in Figure 4. It is obvious that all tetragonal compounds contain a large amount of Yb^{3+} (~75%), similar to pure YbC_2 (81% Yb^{3+}).[17] In contrast, all monoclinic

dx.doi.org/10.1021/ic400531j | Inorg. Chem. 2013, 52, 7020−7030

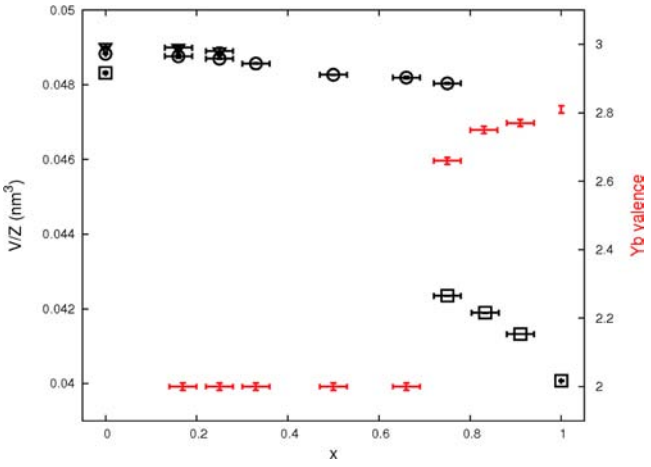

Figure 4. Comparison of unit cell volume (black) and Yb valence (red) in $Yb_xCa_{1-x}C_2$. The different crystal structures of the compounds are marked with symbols: CaC_2 type structure (□), ThC_2 type structure (○), and CaC_2-III type structure (▽).

compounds exclusively contain Yb^{2+}. Unit cell volume and Yb valence show an inverted behavior clearly reflecting their close correlation.

As $Yb_{0.75}Ca_{0.25}C_2$ shows a coexistence of 89% CaC_2 type structure and 11% ThC_2 type structure, the obtained mean valence of 2.66 has to be regarded as an averaged value for both phases. Moreover, this value can be calculated correctly by assuming 11% Yb^{2+} (ThC_2 type structure) and 89% Yb in a mixed-valence state with ~75% Yb^{3+} (CaC_2 type structure).

Obviously, the crystal structure changes in $Yb_xCa_{1-x}C_2$, caused by a variation of the composition x, lead to a valence change from mixed-valent behavior in tetragonal compounds to pure divalent Yb in monoclinic compounds. The Yb^{2+} cation seems to prefer the ThC_2 type structure. Actually, this structure type has only been observed for divalent dicarbides (BaC_2, SrC_2, CaC_2, and EuC_2)[16,21−23] and tetravalent dicarbides (e.g., ThC_2)[36,37] up to now. For trivalent dicarbides the ThC_2 type structure is unknown. As a result, the monoclinic compounds of the solid solution $Yb_xCa_{1-x}C_2$ resemble EuC_2. Like EuC_2 they appear as black powders, whereas YbC_2, the tetragonal compounds of the solid solution $Yb_xCa_{1-x}C_2$, and all other LnC_2 show a metallic luster. Unfortunately, measurements of the electrical conductivity on pressed pellets of selected samples did not lead to reliable results, most likely due to problems contacting the pellets properly.

Structural Investigations at High and Low Temperatures. Our findings at room temperature clearly show the pronounced structure dependence of the Yb valence in the solid solution $Yb_xCa_{1-x}C_2$. The occurrence of three different structure types leads to the question of whether $Yb_xCa_{1-x}C_2$ compounds also show a distinct temperature dependent polymorphism as observed for the alkaline earth metal carbides AEC_2.[21−23] If so, temperature dependent phase transitions should result in temperature dependent Yb valence changes, if the crystal structure transforms from the tetragonal to one of the monoclinic structures and vice versa. Therefore, we explored the temperature dependent phase diagram of $Yb_xCa_{1-x}C_2$ by means of synchrotron and neutron powder diffraction.

$Yb_{0.75}Ca_{0.25}C_2$ may be regarded as the most interesting compound of the series, as it already shows a coexistence of ThC_2 type structure and CaC_2 type structure at room temperature. It was therefore investigated by both synchrotron and neutron TOF powder diffraction. As a large amount of the compound was required for neutron diffraction, different batches were used for both diffraction techniques. In contrast to the X-ray sample (see Table 1), the neutron sample showed a different phase ratio of modifications in the CaC_2 (97.5%) and the ThC_2 (2.5%) type structures at room temperature. An explanation for this difference will be presented in the course of the following discussion.

For the neutron diffraction data it was possible to refine the mixed site occupancies of calcium and ytterbium. For example, the refinement of the 300 K data of $Yb_{0.67}Ca_{0.33}C_2$ and $Yb_{0.75}Ca_{0.25}C_2$ (Figures S13 and S14 in the Supporting Information) gave the Yb:Ca compositions 0.690(6):0.310(6) and 0.743(5):0.257(5), respectively. These results confirm an excellent agreement between the nominal and the refined composition. Therefore, in all refinements the nominal composition was used, as it led to a much faster convergence. Temperature dependent TOF neutron powder diffraction experiments revealed an unusual phase behavior of $Yb_{0.75}Ca_{0.25}C_2$. In the temperature range 400−600 K the tetragonal CaC_2 type structure continuously transforms to the monoclinic ThC_2 type structure (Figure 5). The ThC_2 type

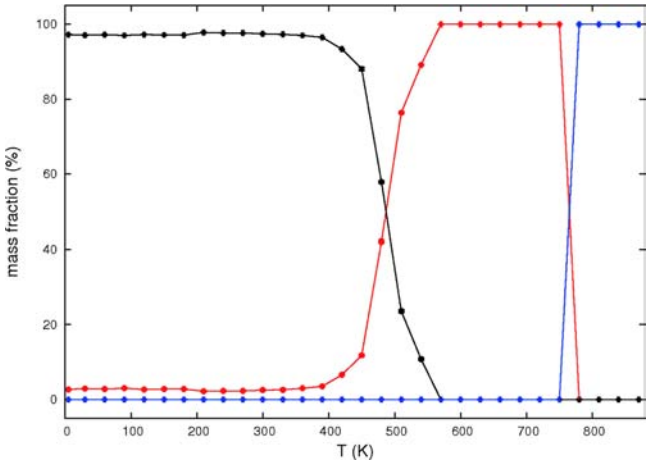

Figure 5. Mass fraction of the different modifications of $Yb_{0.75}Ca_{0.25}C_2$ as a function of temperature, obtained from Rietveld refinements with neutron TOF powder diffraction data: CaC_2 type structure (black), ThC_2 type structure (red), and CaC_2-IV type structure (blue).

structure can therefore be regarded as the modification being more stable than the CaC_2 type structure at these temperatures. This observation is remarkable, as the ThC_2 type structure has never been observed as being more stable than the CaC_2 type structure at elevated temperatures before. For all AEC_2 compounds (and for EuC_2 as well) the CaC_2 type structure is the thermodynamically stable modification at elevated temperatures, whereas the ThC_2 type structure is more stable at lower temperatures.[16,21−23] At about 750 K a sharp transition to the cubic high temperature modification (CaC_2-IV type structure, $Fm\bar{3}m$, $Z = 4$) is observed, which is also known for the binary compounds CaC_2 and YbC_2.[17,21] At low temperatures a complete transformation to the CaC_2 type structure has not been observed; the phase ratio remains constant with a mass fraction of ~97.5% CaC_2 type structure down to 5 K. Hence, this phase transformation seems to be inhibited kinetically at temperatures below ~400 K. These findings may also explain the different room temperature phase ratios of

dx.doi.org/10.1021/ic400531j | Inorg. Chem. 2013, 52, 7020−7030

samples used for synchrotron and neutron diffraction experiments (cf. Figures 5 and S3, Supporting Information). As the reaction conditions, especially the cooling procedure, are not completely reproducible, the transformation rate upon cooling may vary for different batches.

Looking at the unit cell volumes obtained by Rietveld refinements with the TOF neutron data, the large volume difference between the tetragonal phase on the one hand and the monoclinic as well as the cubic phase on the other hand is remarkable (Figure 6). As was shown in the previous

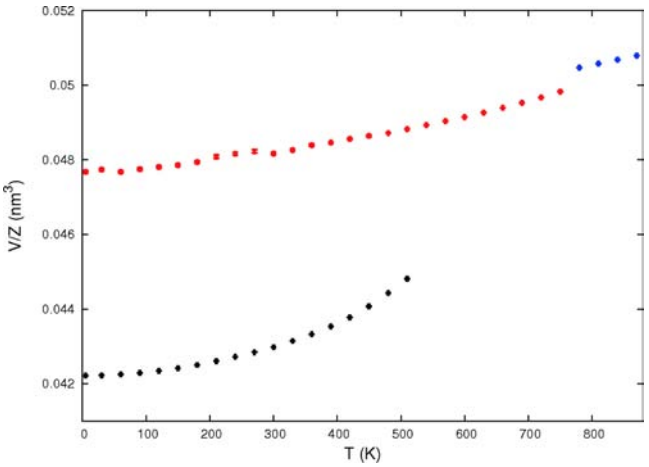

Figure 6. Unit cell volume per formula unit of the different modifications of $Yb_{0.75}Ca_{0.25}C_2$ as a function of temperature, obtained from Rietveld refinements with neutron TOF powder diffraction data: CaC_2 type structure (black), ThC_2 type structure (red), and CaC_2-IV type structure (blue).

discussion, the volume difference between the tetragonal and the monoclinic modification is caused by different Yb valence states. Since the normalized volumes of the monoclinic phase and the cubic phase only differ by 1.3%, a value frequently found for first order phase transitions, it is self-evident to conclude that the cubic phase also contains exclusively Yb^{2+} cations. This suggestion will be proved by means of HERFD-XANES spectroscopic investigations, described below. The finding that only one cubic high temperature modification is observed supports our assumption that the tetragonal and the monoclinic modification have the same composition.

Besides providing structural information, neutron powder diffraction data also allow for some complementary information about the Yb valence states in dicarbide compounds by analyzing the C−C bond length within the C_2 dumbbells. The occupancy of the conduction band in trivalent compounds results in a C−C distance of ∼129 pm (bond order BO = 2.5) at room temperature,[18] whereas divalent compounds show a C−C distance of ∼120 pm (bond order BO = 3.0) comparable to acetylene.[22] We therefore determined the C−C bond length of the different modifications in $Yb_{0.75}Ca_{0.25}C_2$ as a function of temperature from Rietveld refinements of the neutron TOF powder data to support our results obtained from HERFD-XANES spectroscopy. Unfortunately, a reasonable refinement of the carbon positions could only be achieved for mass fractions of the respective phases larger than 50%. A simultaneous refinement of both phases was therefore only possible at T = 480 K (compare Figure 5).

Figure 7 shows the results of the determination of the C−C bond lengths. At low temperatures the tetragonal modification

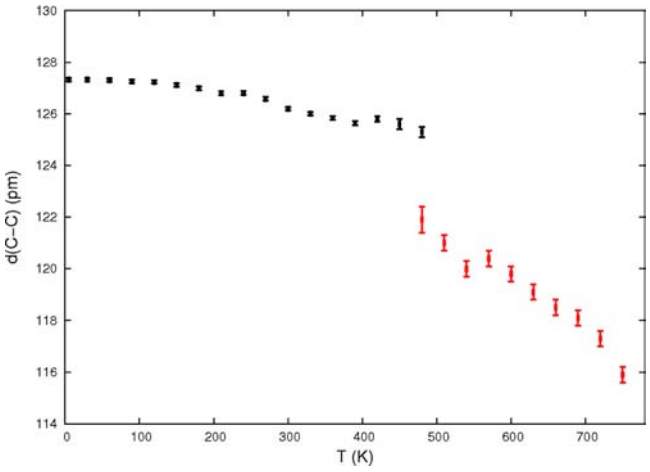

Figure 7. C−C bond lengths of the different modifications in $Yb_{0.75}Ca_{0.25}C_2$ as a function of temperature, obtained from Rietveld refinements of neutron TOF powder diffraction data: CaC_2 type structure (black) and ThC_2 type structure (red).

contains C−C dumbbells with a C−C distance of 127.33(6) pm, similar to pure YbC_2 (d(C−C) = 128.42(2) pm).[17,18] With increasing temperature a significant decrease of the C−C distance is observed for the tetragonal modification: at 480 K it has been reduced to 125.3(3) pm. This behavior has also been observed for alkaline earth metal dicarbides and can be explained by the increasing thermal motion of the C_2 dumbbells around their center of gravity with increasing temperature.[22] The monoclinic modification shows a similar trend: its C−C bond length decreases from 121.9(5) pm at 480 K to 115.9(3) pm at 750 K. But obviously, there is a significant step between the curves of both modifications, showing a bond length difference of 3.4 pm at T = 480 K. This significant difference of the C−C distances of both modifications clearly indicates a different Yb valence state. However, quantitative information cannot be extracted from these results, as the C−C bond lengths cannot be assigned explicitly to a specific Yb valence state.

Among the remaining members of the solid solution $Yb_xCa_{1-x}C_2$, the compound $Yb_{0.91}Ca_{0.09}C_2$ also shows an interesting phase behavior. Although it contains only 9% calcium atoms, its structural behavior, analyzed with synchrotron powder diffraction techniques, differs significantly from pure YbC_2. At RT it crystallizes, like pure YbC_2, in the tetragonal CaC_2 type structure; at higher temperatures the powder patterns reveal a transformation to the cubic high temperature modification (CaC_2-IV type structure). But different to YbC_2, this transformation occurs at a much lower transition temperature T_{Ph} = 773 K ($T_{Ph}(YbC_2)$ = 1023 K). Furthermore, the phase transition is not sharp but diffuse: CaC_2 type structure and CaC_2-IV type structure coexist in a wide temperature range from 773 to 973 K (Figure 8). At 973 K, the maximum temperature of the measurement, the transformation is still not complete: 18% of the compound remains in the tetragonal structure. Remarkably, the unit cell volumes of the two phases, obtained from Rietveld refinements with synchrotron powder diffraction data, differ very much accounting for a relative difference of 16% (Figure S2, Supporting Information). Again, different Yb valence states can be assumed in both modifications, as will be proved by means of HERFD-XANES spectroscopy, described below.

dx.doi.org/10.1021/ic400531j | Inorg. Chem. 2013, 52, 7020−7030

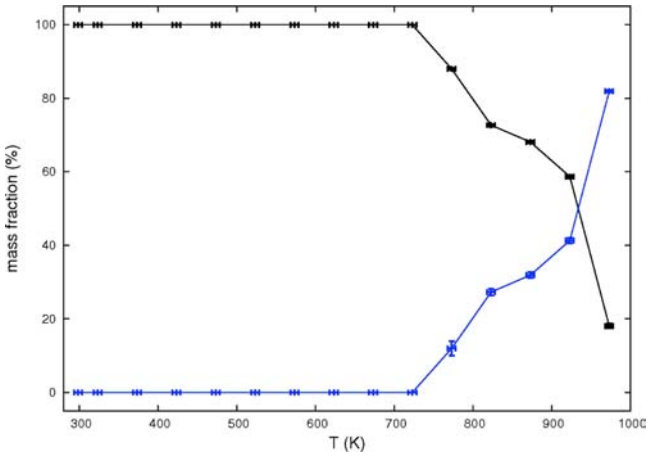

Figure 8. Mass fraction of the different modifications of $Yb_{0.91}Ca_{0.09}C_2$ as a function of temperature, obtained from Rietveld refinements with synchrotron powder diffraction data: CaC_2 type structure (black) and CaC_2-IV type structure (blue).

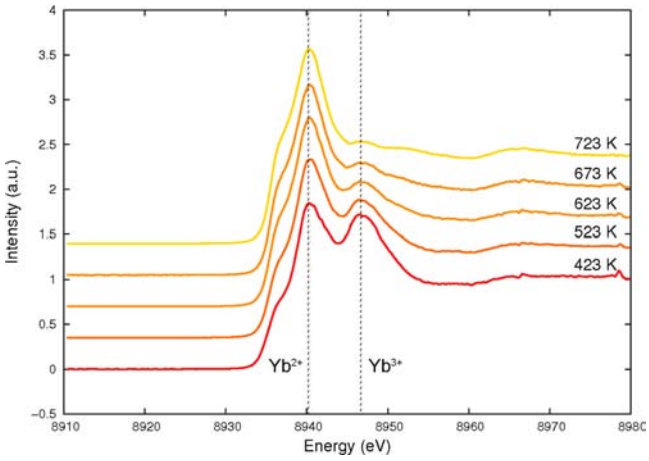

Figure 9. Yb L_{III} HERFD-XANES spectra of $Yb_{0.75}Ca_{0.25}C_2$ at five different temperatures. Dotted lines indicate the approximate positions of the white lines for Yb^{2+} and Yb^{3+} ions.

HERFD-XANES Spectroscopy at High and Low Temperatures. The interesting phase behavior of several compounds of the $Yb_xCa_{1-x}C_2$ series at high and low temperatures, accompanied by large unit cell volume differences between the occurring crystal structures, points to Yb valence changes. To verify this assumption, temperature dependent HERFD-XANES spectroscopic investigations were performed at beamline ID26 (ESRF).

At first, $Yb_{0.75}Ca_{0.25}C_2$ was investigated at temperatures between 15 and 873 K using the same sample that was used for the synchrotron powder diffraction experiments. Spectra were only recorded during the heating process. The reversibility of occurring changes was finally checked by a second measurement at the starting temperature after cooling.

The collected data at low temperatures do not show a significant change of the white lines pointing to a constant mean valence state down to 15 K (Figure S18, Supporting Information). These observations are in perfect agreement with the results of the neutron TOF powder diffraction experiments that revealed a kinetic inhibition of the phase transformation between CaC_2 and ThC_2 type structure below 400 K. According to our assumption that different valence states are stabilized in the two modifications, a constant Yb valence state is therefore in good agreement with a constant phase ratio. However, at high temperatures the XANES spectra show remarkable changes (Figure 9). The quantitative analysis of the spectra by means of least-squares fitting (as an example of the fits see Figure S15 in the Supporting Information) reveals a continuous decrease of the Yb valence state starting at T = 473 K and ending at T = 723 K with a final mean Yb valence of 2.0. A comparison with the structural data obtained from synchrotron powder diffraction experiments reveals a perfect correlation between Yb valence states and the occurring crystal structures (Figure 10). From 450 K up to 748 K a slow transformation from the CaC_2 type structure to the ThC_2 type structure is observed, which leads to a decrease of the Yb valence. Assuming that in the ThC_2 type structure an Yb valence of +2 is preferred and in the CaC_2 type structure an Yb valence of +2.75 (see above), the temperature dependence of the Yb valence can be perfectly calculated from the phase fractions of the different modifications (Figure S19 in the Supporting Information). At 748 K a sharp phase transition to

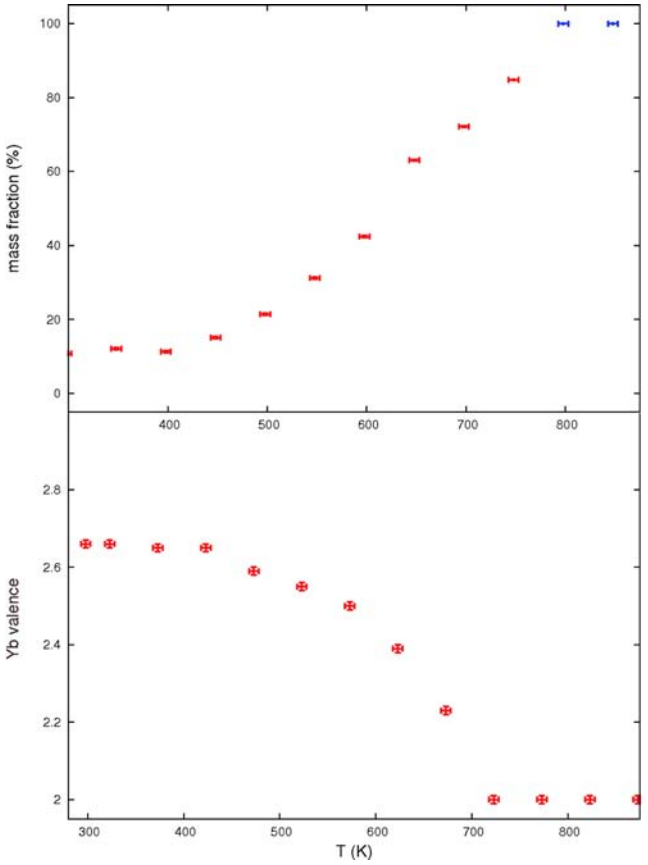

Figure 10. Mass fraction of ThC_2 type structure (red) and CaC_2-IV type structure (blue, upper chart) in comparison to the Yb valence (red, lower chart) of $Yb_{0.75}Ca_{0.25}C_2$ as a function of temperature.

the cubic high temperature modification CaC_2-IV is visible in the diffraction patterns. As the Yb valence obtained from the HERFD-XANES spectra remains at a constant value of 2.0 up to 873 K, the spectroscopic investigations clearly prove that the cubic modification also contains exclusively Yb^{2+} ions.

Similar results are obtained for $Yb_{0.91}Ca_{0.09}C_2$, investigated in the temperature range 15−1073 K. Again, measurements were performed only during the heating process. The reversibility was checked by a second measurement after cooling at the

dx.doi.org/10.1021/ic400531j | Inorg. Chem. 2013, 52, 7020−7030

starting temperature. Comparable to $Yb_{0.75}Ca_{0.25}C_2$, the XANES spectra at low temperatures do not indicate any valence changes of the Yb ion (Figure S16, Supporting Information). However, at high temperatures a significant valence change is observed in the HERFD-XANES spectra (Figure S17, Supporting Information). Starting at a temperature of 773 K the Yb valence decreases continuously from a mean value of 2.73 to 2.0 at 1073 K (Figure 11). Again, Yb

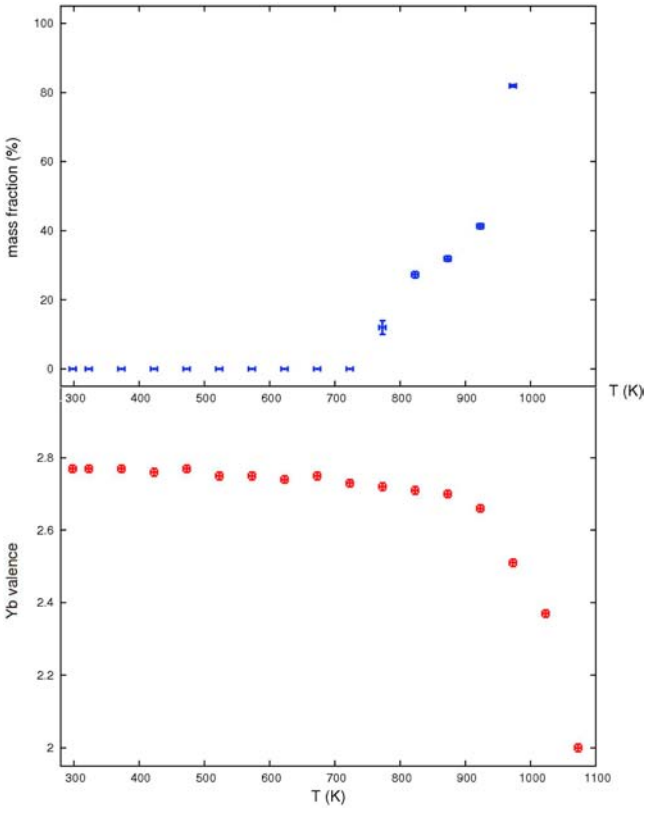

Figure 11. Mass fraction of CaC_2-IV type structure (blue, upper chart) in comparison to the Yb valence (red, lower chart) of $Yb_{0.91}Ca_{0.09}C_2$ as a function of temperature.

valence state and occurring crystal structures are strongly correlated, as an increase of the phase fraction of the cubic CaC_2-IV type structure is accompanied by a decrease of the Yb valence state. The HERFD-XANES data unambiguously prove the existence of Yb^{2+} ions in the cubic modification of $Yb_{0.91}Ca_{0.09}C_2$.

DSC Measurements for Determination of Lattice Strain. The previous results clearly prove that crystal structures and Yb valence states are closely correlated in the solid solution $Yb_xCa_{1-x}C_2$. These findings can be further corroborated by using the "Lattice Strain Theory" of McColm et al., who carried out extensive studies on $Ln_xLn'_{1-x}C_2$ (Ln, Ln′ = lanthanide metal) solid solutions.[38,39]

As already described for $Ln_xLn'_{1-x}C_2$ solid solutions, a determination of the transition temperature to the cubic high temperature modification in the CaC_2-IV type structure provides a direct insight into the lattice strain of the tetragonal and monoclinic modifications.[38−43] The main difference between the cubic phase and all other existing modifications is the alignment of the C_2 dumbbells. While these dumbbells are aligned in a fixed direction in the tetragonal and monoclinic modifications, they show a disordered orientation in the cubic high temperature modification. Therefore, a transition from cubic to tetragonal or monoclinic modifications requires attractive interactions between C_2 dumbbells and metal cations that depend on the charge density of the cations and therefore on their electric charge and ionic radii.[39] Hence, an exchange of the cation has a direct influence on the transition temperature and the heat of transition.[39]

Looking at the mixed occupancy in solid solutions, one would expect a linear relationship of the transition temperature and the heat of transition on x between the two boundary compounds with $x = 0$ and $x = 1$. In fact, this is only the case for cations that show comparable interactions with the C_2 dumbbells.[24,38,39,41] A significant lattice strain that should be proportional to the differences in the ionic radii as well as to the amount of mixing with a theoretical maximum at $x = 0.5$ reduces the expected values, because a concerted alignment of the C_2 dumbbells gets hampered by different cations in the dumbbell's immediate crystallographic surrounding.[39] Therefore, a characteristic minimum of the transition temperatures occurs, whose value mainly depends on the differences of the cations' radii.[38,39,41]

As the ionic radius of Ca^{2+} (114 pm, CN = 10) is much more similar to Yb^{2+} (112 pm, CN = 10) than to Yb^{3+} (100 pm, CN = 10),[25] only the latter should produce a significant lattice strain in terms of McColm's theory. It should therefore be possible to identify different valence states of Yb by analyzing the transition temperatures and heats of transition of the solid solution $Yb_xCa_{1-x}C_2$.

To corroborate our findings from diffraction and spectroscopic investigations we studied the high temperature phase transition of all synthesized compounds by DSC measurements. All samples, including the pure dicarbides YbC_2 and CaC_2, were investigated in the temperature range 298−873 K; for $x > 0.83$ the maximum temperature was increased to 1073 K.

Figure 12 shows the results of all DSC measurements upon heating. Most compounds show a sharp endothermic signal

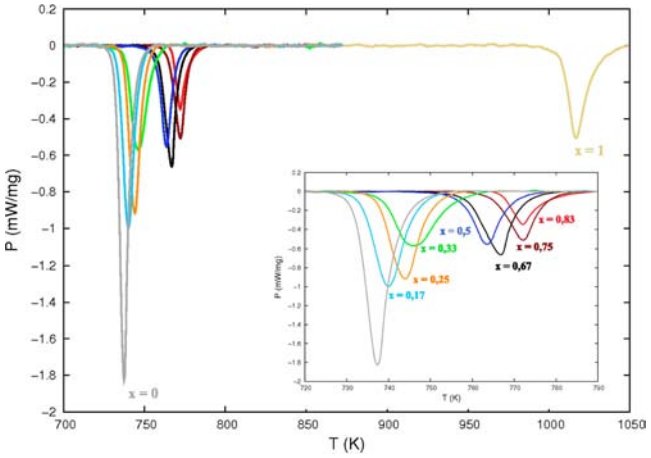

Figure 12. DSC plots of the solid solution $Yb_xCa_{1-x}C_2$ upon heating (background corrected). Details in the temperature range 720−790 K are shown in the inset.

that can be assigned to the discussed high temperature phase transition. As the transition between CaC_2 and ThC_2 type structures can be regarded as a displacive transformation in the second coordination sphere, it does not show an observable evolution of heat and is therefore not detectable in the DSC. The only compound without any detectable signal at all is

dx.doi.org/10.1021/ic400531j | Inorg. Chem. 2013, 52, 7020−7030

$Yb_{0.91}Ca_{0.09}C_2$. This finding can be explained by the results of the diffraction experiments of its high temperature phase transition (Figure 8). They reveal a slow continuous phase transition to the CaC_2-IV type structure in a wide temperature range. Therefore, the heat of transition detectable by DSC is smeared out in this wide temperature range and vanishes in the background signal.

The curves obtained upon cooling revealed a complete reversibility of the observed phase transitions (e.g., Figure S20, Supporting Information). The following analysis was therefore restricted to the heating data.

In a first step we extracted the phase transition temperatures T_{Ph} from the DSC data. The results plotted as a function of the composition x are shown in Figure 13. Obviously all solid

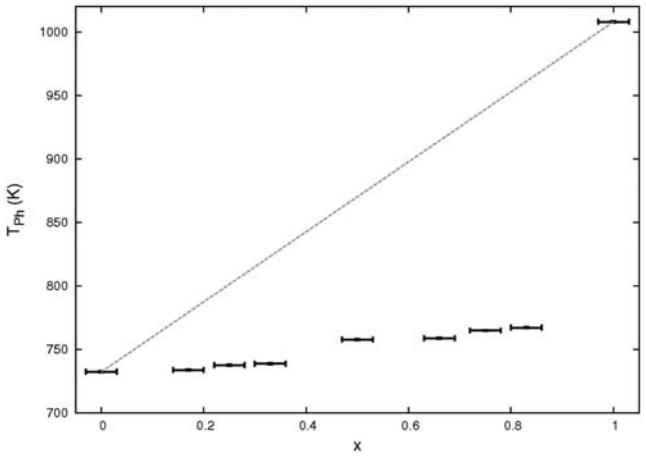

Figure 13. Transition temperatures T_{Ph} of $Yb_xCa_{1-x}C_2$ as a function of the composition x. The hypothetical behavior of an "ideal" solid solution is plotted as a dotted line.

solutions show a comparable transition temperature similar to that of pure CaC_2 (T_{ph} = 732.3 K). For large lattice strains a decrease of the transition temperatures even below the value of pure CaC_2 is expected, as described by McColm and Adachi.[38−41] Our data therefore suggest only a small lattice strain indicating Yb^{2+} cations, which have ionic radii similar to Ca^{2+}. To gather more information from the DSC data we extracted the heat of transition ΔH_{Ph} by determining the area A of the DSC peaks. Subsequently, the lattice strain energy E_S can be calculated by

$$E_S = \Delta H_{Ph,obs} - \Delta H_{Ph,theo}$$

where $\Delta H_{Ph,obs}$ is the observed heat of transition and $\Delta H_{Ph,theo}$ is the hypothetical heat of transition as obtained from a straight line between x = 0 and x = 1. The results are shown in Figure 14.

As can be seen in Figure 14, bottom, all strain energies for compounds with x < 0.75 can be described by a simple Gaussian function with its maximum at x = 0.5, typical for dicarbide solid solutions with a constant cation valence over the whole composition range.[38−41] A further comparison with other dicarbide solid solutions shows that the respective maximum strain energy E_S = 3.3 kJ/mol is indeed very small: For $La_xGd_{1-x}C_2$ a maximum strain energy E_S = 13.88 kJ/mol was reported.[40] In the latter the cations have a relative difference of their ionic radii of $\Delta R/R$ = 9.5%. In contrast, $La_xCe_{1-x}C_2$ solid solutions contain cations with $\Delta R/R$ = 1.7%. Consequently, the maximum strain energy was determined as

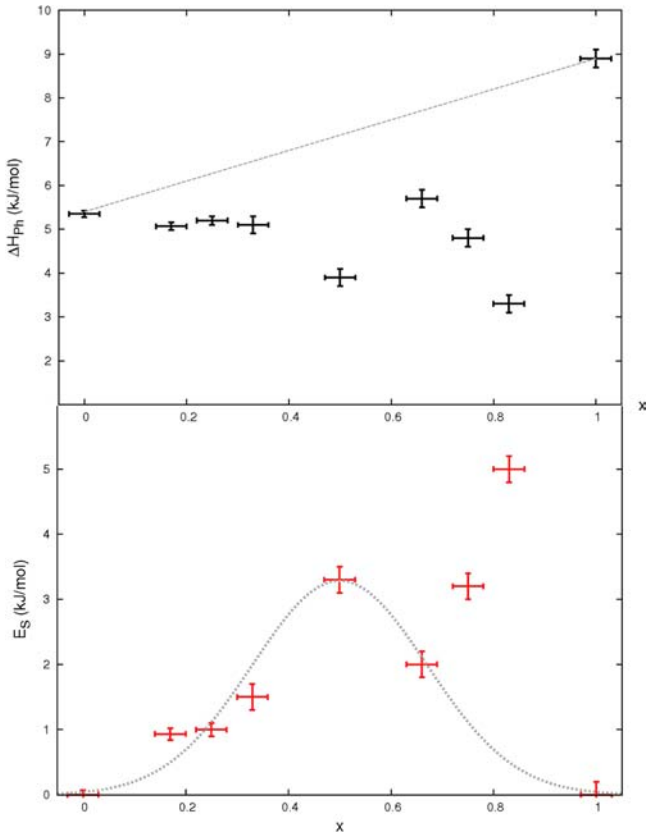

Figure 14. Heats of transition (black) and lattice strain energies (red) of $Yb_xCa_{1-x}C_2$ as a function of the composition x. The expected behavior for an "ideal" solid solution with similar cations ($\Delta R/R$ = 0%, comparable interactions with the C_2 dumbbells) are plotted as a dotted line (top). The dotted Gaussian function describes the estimated trend of the lattice strain energies in case of a constant Yb valence (bottom).

E_S = 2.1 kJ/mol.[43] Therefore, one can conclude that all compounds $Yb_xCa_{1-x}C_2$ with x < 0.75 contain Yb^{2+} that does not produce a large lattice strain.

Furthermore, compounds with $x \geq 0.75$ show a considerable deviation from the simple Gaussian trend. For these compounds significantly higher lattice strain energies with a maximum of E_S = 5 kJ/mol for x = 0.83 are obtained. This points to Yb^{3+} cations, which should produce a higher lattice strain.

So all findings about the Yb valence state in the solid solution $Yb_xCa_{1-x}C_2$ obtained by analysis of HERFD-XANES data are therefore in excellent agreement with those obtained by investigation of lattice strain energies from DSC experiments.

CONCLUSION

We were able to synthesize the solid solution $Yb_xCa_{1-x}C_2$ with $0 \leq x \leq 1$. Its complex phase behavior was investigated by neutron and synchrotron powder diffraction. Four different structure modifications ($I4/mmm$, Z = 2; $C2/c$, Z = 4; $C2/m$, Z = 4; $Fm\bar{3}m$, Z =4) were found depending upon the temperature and the composition x. Most interestingly, at room temperature a large volume decrease ($\Delta V/V \approx 12\%$) with increasing x was found (Figure 2). HERFD-XANES data confirmed our first assumption that a valence change from Yb^{2+} to Yb^{3+} is responsible for this behavior. This assumption is also corroborated by measurements of the magnetic susceptibilities. Selected measurements are given in the Supporting Informa-

dx.doi.org/10.1021/ic400531j | Inorg. Chem. 2013, 52, 7020−7030

tion (Figures S21 and S22). For x = 0.75 two modifications coexist at room temperature. From a combination of diffraction and XANES experiments it was shown that in the monoclinic ThC_2 type structure ($C2/c$, Z = 4) divalent Yb^{2+} is preferred, whereas in the tetragonal CaC_2 type structure ($I4/mmm$, Z = 2) a Yb valence similar to that in YbC_2 (~+2.75) is found. As the ratio of both modifications changes with temperature, the mean Yb valence determined by XANES spectroscopy can be calculated from this ratio. Thus, a rather complex dependence of the Yb valence is found that is influenced by temperature, composition, and crystal structure. In Figure 15 this dependence is schematically summarized. An explanation for these valence changes cannot be given at the moment, but obviously the different radii of Ca^{2+}, Yb^{2+}, and Yb^{3+} play a crucial role. It is evident that a more detailed (theoretical) analysis of our results is needed.

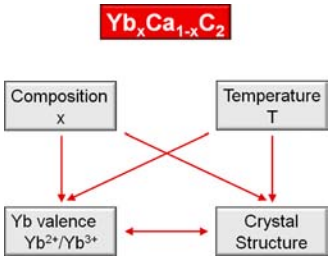

Figure 15. Schematic presentation of the complex valence changes observed in the solid solution $Yb_xCa_{1-x}C_2$.

Temperature and pressure induced Yb valence changes are found quite frequently, but to our knowledge structure induced valence changes are rare. They have been discussed for Eu doped BaB_8O_{13}[44] and EuH_x.[45] For the latter the Eu valence changes were induced by application of H_2 under high pressure.

It is interesting to mention that all LnC_2 compounds containing trivalent Ln^{3+} (Ln = La–Lu except Eu) crystallize in the tetragonal CaC_2 type structure. EuC_2, however, which contains divalent Eu^{2+}, crystallizes in the monoclinic ThC_2 type structure.[16,46] Thus, this behavior is very similar to the structure-valence dependence we found in the solid solution $Yb_xCa_{1-x}C_2$.

In the Article, we have only discussed the valence changes of two members of the solid solution $Yb_xCa_{1-x}C_2$ with x = 0.75 and 0.91. For the other compositions, results are obtained which are in agreement with the concept described above.

In the meantime we have been able to synthesize several other solid solutions of YbC_2 with alkaline earth metal carbides AEC_2 (AE = Ca–Ba) or EuC_2. They show a behavior very similar to that of $Yb_xCa_{1-x}C_2$. Details are still under investigation. For solid solutions of EuC_2 with AEC_2, however, no changes from divalent europium have been observed up to now (for AE = Sr see ref 24). But it seems to be worthwhile to investigate these systems under pressure.

■ ASSOCIATED CONTENT

Supporting Information

Additional data and results of synchrotron and neutron powder diffraction experiments, HERFD-XANES spectra, DSC investigations, and magnetic susceptibility measurements. This material is available free of charge via the Internet at http://pubs.acs.org.

■ AUTHOR INFORMATION

Corresponding Author

*E-mail: Uwe.Ruschewitz@uni-koeln.de.

Notes

The authors declare no competing financial interest.

■ ACKNOWLEDGMENTS

We are grateful to the technical support staff at the ESRF and HASYLAB for the assistance during the experiment as well as Peter Kliesen for recording the DSC scans and Oliver Heyer for measurements of the magnetic susceptibilities. Experiments at the ISIS Pulsed Neutron and Muon Source were supported by a beamtime allocation from the Science and Technology Facilities Council. We thank the German Research Foundation (DFG) for financial support (SPP 1166, RU 546/8-1).

■ REFERENCES

(1) Jayaraman, A. *Angew. Chem.* **1980**, *92*, 626.
(2) Lossau, N.; Kierspel, H.; Langen, J.; Schlabitz, W.; Wohlleben, D.; Mewis, A.; Sauer, Ch. *Z. Phys. B: Condens. Matter* **1989**, *74*, 227.
(3) Cho, B. K.; DiSalvo, F. J.; Kim, J. S.; Stewart, G. R.; Bud'ko, S. L. *Physica B* **1998**, *253*, 40.
(4) Fuse, A.; Nakamoto, G.; Kuriso, M.; Ishimatsu, N.; Tanida, H. *J. Alloys Compd.* **2004**, *376*, 34.
(5) Annese, E.; Rueff, J.-P.; Vankó, G.; Grioni, M.; Braicovich, L.; Degiorgi, L.; Gusmeroli, R.; Dallera, C. *Phys. Rev. B* **2004**, *70*, 075117.
(6) Gumeniuk, R.; Bischoff, E.; Burkhardt, U.; Prots, Yu.; Schnelle, W.; Vasylechko, L.; Schmidt, M.; Kuzma, Yu.; Grin, Yu. *J. Solid State Chem.* **2009**, *182*, 3374.
(7) Yamaoka, H.; Jarrige, I.; Tsujii, N.; Imai, M.; Lin, J.-F.; Matsunami, M.; Eguchi, R.; Arita, M.; Namatame, H.; Taniguchi, M.; Taguchi, M.; Senba, Y. *Phys. Rev. B* **2011**, *83*, 104525.
(8) Arvanitidis, J.; Papagelis, K.; Margadonna, S.; Prassides, K.; Fitch, A. N. *Nature* **2003**, *425*, 599.
(9) Margadonna, S.; Arvanitidis, J.; Papagelis, K.; Prassides, K. *Chem. Mater.* **2005**, *17*, 4474.
(10) Spedding, F. H.; Gschneidner, K., Jr.; Daane, A. H. *J. Am. Chem. Soc.* **1958**, *80*, 4499.
(11) Sakai, T.; Adachi, G.; Yoshida, T.; Shiokawa, J. *J. Chem. Phys.* **1981**, *75*, 3027.
(12) Vickery, R. C.; Sedlacek, R.; Ruben, A. *J. Chem. Soc.* **1959**, 498.
(13) Vickery, R. C.; Sedlacek, R.; Ruben, A. *J. Chem. Soc.* **1959**, 503.
(14) Vickery, R. C.; Sedlacek, R.; Ruben, A. *J. Chem. Soc.* **1959**, 505.
(15) Sakai, T.; Adachi, G.; Yoshida, T.; Shiokawa, J. *J. Less-Common Met.* **1981**, *81*, 91.
(16) Wandner, D.; Link, P.; Heyer, O.; Mydosh, J.; Ahmida, M. A.; Abd-Elmeguid, M. M.; Speldrich, M.; Lueken, H.; Ruschewitz, U. *Inorg. Chem.* **2010**, *49*, 312; *Inorg. Chem.* **2011**, *50*, 2703.
(17) Link, P.; Glatzel, P.; Kvashnina, K.; Smith, R. I.; Ruschewitz, U. *Inorg. Chem.* **2011**, *50*, 5587.
(18) Atoji, M. *J. Chem. Phys.* **1961**, *35*, 1950.
(19) Atoji, M.; Flowers, R. H. *J. Chem. Phys.* **1970**, *52*, 6430.
(20) Sales, B. C.; Wohlleben, D. K. *Phys. Rev. Lett.* **1975**, *35*, 1240.
(21) Knapp, M.; Ruschewitz, U. *Chem.—Eur. J.* **2001**, *7*, 874.
(22) Vohn, V.; Kockelmann, W.; Ruschewitz, U. *J. Alloys Compd.* **1999**, *284*, 132.
(23) Vohn, V.; Knapp, M.; Ruschewitz, U. *J. Solid State Chem.* **2000**, *151*, 111.
(24) Link, P.; Wandner, D.; Schellenberg, I.; Pöttgen, R.; Paulus, M.; Sahle, C. J.; Sternemann, C.; Ruschewitz, U. *Z. Anorg. Allg. Chem.* **2010**, *636*, 2276.
(25) Lide, D. R. *CRC Handbook of Chemistry and Physics*, 81st ed.; CRC Press: Boca Raton, FL, 2000.
(26) Knapp, M.; Joco, V.; Baehtz, C.; Bercht, H. H.; Berghaeuser, A.; Ehrenberg, H.; von Seggern, H.; Fuess, H. *Nucl. Instrum. Methods Phys. Res., Sect. A* **2004**, *521*, 565.

(27) *STOE WinXPow. Version 1.07*; STOE & Cie GmbH: Darmstadt, Germany, 2000.
(28) Larson, A. C.; von Dreele, R. B. *Los Alamos Natl. Lab., [Rep.] LA-UR (U.S.)* **1987**, *86*, 748 , revised PC version of November 2001.
(29) Smith, R. I.; Hull, S.; Armstrong, A. R. *Mater. Sci. Forum* **1994**, *166−169*, 251.
(30) Gauthier, C.; Solé, V.; Signorato, R.; Goulon, J.; Moguiline, E. *J. Synchrotron Radiat.* **1999**, *6*, 164.
(31) Newville, M. *IFEFFIT, version 1.2.11c*; University of Chicago: Chicago, IL, 2008.
(32) *GNUPLOT, version 4.4.0*, open source. http://gnuplot.sourceforge.net/.
(33) *NETSCH Proteus-thermal analysis, version 4.8.5*; NETZSCH-Gerätebau GmbH: Selb, Germany, 1999−2008.
(34) Glaser, J.; Dill, S.; Marzini, M.; Mayer, H. A.; Meyer, H.-J. *Z. Anorg. Allg. Chem.* **2001**, *627*, 1090.
(35) Kvashnina, K. O.; Butorin, S. M.; Glatzel, P. *J. Anal. At. Spectrom.* **2011**, *26*, 1265.
(36) Jones, D. W.; McColm, I. J.; Steadman, R.; Yerkess, J. *J. Solid State Chem.* **1987**, *68*, 219.
(37) Bowman, A. L.; Krikorian, N. H.; Arnold, G. P.; Wallace, T. C.; Nereson, N. G. *Acta Crystallogr., Sect. B.* **1968**, *24*, 1121.
(38) McColm, I. J.; Colquhoun, I.; Clark, N. J. *J. Inorg. Nucl. Chem.* **1972**, *34*, 3809.
(39) McColm, I. J.; Quigley, T. A.; Clark, N. J. *J. Inorg. Nucl. Chem.* **1973**, *35*, 1931.
(40) Low, I. R.; McColm, I. J.; Quigley, T. A. *J. Less-Common Met.* **1976**, *46*, 217.
(41) Adachi, G.; Nishihata, T.; Shiokawa, J. *J. Less-Common Met.* **1973**, *32*, 301.
(42) Adachi, G.; Shibata, Y.; Ueno, K.; Shiokawa, J. *J. Inorg. Nucl. Chem.* **1976**, *38*, 1023.
(43) Adachi, G.; Tonomura, F.; Shibata, Y.; Shiokawa, J. *J. Inorg. Nucl. Chem.* **1978**, *40*, 489.
(44) Machida, K.-I.; Ueda, D.; Inoue, S.; Adachi, G.-Y. *Electrochem. Solid State Lett.* **1999**, *2*, 597.
(45) Matsuoka, T.; Fujihisa, H.; Hirao, N.; Ohishi, Y.; Mitsui, T.; Masuda, R.; Seto, M.; Yoda, Y.; Shimizu, K.; Machida, A.; Aoki, K. *Phys. Rev. Lett.* **2011**, *107*, 025501.
(46) Hülsen, M.; Dolg, M.; Link, P.; Ruschewitz, U. *Theor. Chem. Acc.* **2011**, *129*, 367.